Chemical Engineering Journal 450 (2022) 138214

Contents lists available at ScienceDirect

Chemical Engineering Journal

journal homepage: www.elsevier.com/locate/cej

Mixed-ligand metal–organic frameworks with coordinatively un-saturated Co(II) and Ni(II) sites for regenerable O_2-selective ad-sorption over N_2

Hanbang Liu [a,b], Liping Yang [a,b], Danhua Yuan [a], Guangye Liu [a], Jiacheng Xing [a], Yunpeng Xu [a,*], Zhongmin Liu [a,b]

[a] National Engineering Research Center of Lower-Carbon Catalysis Technology, Dalian National Laboratory for Clean Energy, Dalian Institute of Chemical Physics, Chinese Academy of Sciences, Dalian 116023, PR China
[b] University of Chinese Academy of Sciences, Beijing 100049, PR China

ARTICLE INFO

Keywords:
O_2-selective adsorbent
O_2/N_2 separation
Metal-organic frameworks
Adsorption selectivity
Regeneration ability

ABSTRACT

For air separation, the separation method relying on adsorbents has attracted wide attention as a low energy consumption process, and the development of O_2-selective adsorbents is of great significance. Metal-organic frameworks with coordinatively unsaturated transition metal sites have great potential in O_2-selective adsorption, but most of them cannot be completely regenerated at ambient temperature or can only be effective at very low temperatures. Herein, we report two mixed-ligand metal–organic framework adsorbents $[M(AIP)(BPY)_{0.5}{\cdot}H_2O]_n{\cdot}2nH_2O$ with coordinatively unsaturated cobalt(II) and nickel(II) sites, which can preferentially adsorb O_2 versus N_2, and their IAST O_2/N_2 selectivities are both significantly greater than 1 at 25 °C. These materials exhibited excellent stability and had no loss of adsorption capacities even after immersion in water for 7 days. More importantly, O_2 adsorption–desorption cycle experiments showed that these adsorbents can be completely regenerated at ambient temperature after adsorbing O_2, and the breakthrough experiments further confirmed their dynamic O_2/N_2 separation potential and regeneration ability. The results of theoretical calculations suggested that the interactions between adsorbents and O_2 are stronger than those of N_2, and they have relatively obvious differences in the N_2 and O_2 interaction energies. This work provides inspirations for searching for metal–organic frameworks that can selectively adsorb O_2 at ambient temperature.

1. Introduction

O_2 is a very important chemical that plays a special role in medicine, chemical manufacturing and the military [1]. In addition, burning fuels containing O_2-enriched air can not only increase energy efficiency but also reduce greenhouse gas emissions [2]. Therefore, it is of great significance to develop a technology that can obtain a large amount of relatively pure O_2 from air. However, as the main component in air, N_2 has a molecular size similar to that of O_2; thus, separating N_2 and O_2 from air is a meaningful and challenging task. In fact, cryogenic distillation based on their different boiling points is the most commonly used method in industry for producing high-purity N_2 and O_2, but it is an energy-intensive process with a huge cost [3–4]. Currently, adsorption and separation processes based on porous adsorbents have become very attractive, such as pressure swing adsorption (PSA), which is a low energy consumption and low-cost process [5]. However, it is worth noting that the purity of O_2 obtained by this method is relatively insufficient compared with cryogenic distillation. For example, the purity of O_2 obtained from the PSA process based on zeolite LiLSX is approximately 90–95 % [6]. Not only LiLSX but also most zeolites are N_2-selective adsorbents that preferentially adsorb N_2 with a high quadrupole moment due to their extraframework cations [5,7–9]. Compared with N_2-selective adsorption, the O_2-selective adsorption process requires fewer adsorbents and shorter packed columns; thus, its equipment investment and energy consumption are lower than those of the N_2-selective adsorption process because O_2 accounts for a much lower proportion of air than N_2 (21 % versus 78 %) [10]. For O_2-selective adsorption, carbon molecular sieves (CMS) are the most common commercial O_2-selective adsorbents for air separation based on kinetic principles, but their pore channels are difficult to control and they do not have significant O_2 selectivity versus N_2 at adsorption equilibrium [7,11–12]. O_2-binding cobalt complexes such as Co(salen) and Co(fluomine) can bind O_2 reversibly and have been tested in air breathing systems, but their commercial applications are limited by their chemical

* Corresponding author.
E-mail address: xuyunpeng@dicp.ac.cn (Y. Xu).

https://doi.org/10.1016/j.cej.2022.138214
Received 8 June 2022; Received in revised form 13 July 2022; Accepted 18 July 2022
Available online 21 July 2022

instability and high cost [13–14]. For traditional zeolite adsorbents, although it has been found that some of them have the ability to selectively adsorb O_2, such as NaUZM-9-H and Ce/NaX, their O_2/N_2 selectivities at ambient temperature are relatively low [15–16].

Metal-organic frameworks (MOFs), a new class of materials with highly crystalline and tunable pore properties, have great potential in gas separation and storage. Many MOFs have demonstrated good performance in separating O_2 and N_2: some MOFs like zeolitic-imidazolate frameworks (ZIFs) can achieve kinetics O_2/N_2 separation through metal and linker replacement [17]; some MOFs with suitable pore size, such as PCN-13, CUK-1, etc., can adsorb more O_2 with smaller size instead of N_2 [18–19]; and some MOFs that interact more strongly with O_2 can also be designed, such as Cu-L_1, Ni-L_1, JLU-Liu18, etc., which can achieve separation by selectively adsorbing O_2 [20–21]. In addition, with the improvement of theoretical calculation and machine learning methods [22–23], it is possible to screen a wide variety of MOFs with O_2/N_2 separation potential, which makes the field of MOFs fruitful. Currently, many MOF materials with coordinatively unsaturated metal sites can bind O_2 and show high selectivities in O_2-selective air separation. For example, Fe_2(dobdc) has high O_2/N_2 selectivity at low temperature, but this O_2-binding performance is irreversible at relatively high temperatures (above −50 °C), and its framework has poor stability in humid environments [24]. Co-BTTri and Co-BDTriP also have high O_2/N_2 selectivities at low temperature, but they all have significantly lower selectivities at 25 °C [25]. Since air separation at ambient temperature consumes less energy than that at low temperature, the development of MOF adsorbents with high O_2 selectivity and good renewability at ambient temperature has become the focus of current research. $Co_2(OH)_2$(BBTA) and Cu(Qc)$_2$ have been found to have high O_2 selectivities at ambient temperature, but their regenerability has not been studied in detail [10,26]. Sc-MIL-100 was found to be a regenerable O_2-selective adsorbent at ambient temperature, but its O_2/N_2 selectivity (1.25, at 25 °C and 100 kPa) was relatively low [27]. Cr_3(btc)$_2$ and Cr-BTT were also reported to be able to selectively adsorb O_2 at ambient temperature, and their O_2/N_2 selectivities were very competitive, but the O_2 uptake on them was reduced as the cycle process was repeated [28–29]. In addition, some theoretical calculations have been carried out to explore and find suitable MOF materials that selectively adsorb O_2 [26,30–31]. The results of theoretical calculations showed that both the coordinatively unsaturated metal sites and the ligands of MOFs can affect their O_2 adsorption performances. MOFs with coordinatively unsaturated early transition metal sites (Ti, V, Cr) were confirmed by calculations to have much stronger interactions with O_2 than N_2, but their strong O_2 binding ability makes them difficult to regenerate. Some other MOFs whose metal sites exhibit relatively mild interactions with O_2, such as cobalt-based MOFs, usually have no O_2 selectivity at ambient temperature if their metal sites bridge weak-field carboxylate-based ligands, such as Co-MOF-74 [25,30]. When some strong-field ligands are used to form cobalt-based MOFs such as Co-BTTri and Co-BDTriP, these MOFs can have strong O_2 affinity [25]. Therefore, suitable metal sites and ligands are the key to developing O_2-selective MOF adsorbents with good selectivity, stability and regenerability at ambient temperature.

In this work, we reported and synthesized two mixed-ligand MOFs $[Co(AIP)(BPY)_{0.5}\cdot H_2O]_n\cdot 2nH_2O$ (Co-AIP-BPY) and $[Ni(AIP)(BPY)_{0.5}\cdot H_2O]_n\cdot 2nH_2O$ (Ni-AIP-BPY) containing different coordinatively unsaturated metal sites, which both used 5-aipaminoisophthalic acid (AIP) and 4,4́-bipyridine (BPY) as ligands. These mixed-ligand MOF materials exhibited special O_2-selective adsorption properties and relatively high O_2/N_2 selectivities, as well as excellent stability and regeneration ability at ambient temperature. The dynamic breakthrough experiments further confirmed their good separation and regeneration performances for the O_2/N_2 mixture. In addition, DFT theoretical calculations showed that the interactions between these materials and O_2 are stronger than those with N_2 but relatively moderate, resulting in excellent O_2-selective adsorption and regeneration performances at ambient temperature.

2. Experimental and methods

2.1. Materials

All reagents and solvents were commercially purchased and used without further purification: cobalt acetate tetrahydrate [Co$(CH_3COO)_2\cdot 4H_2O$, 99.5 %], nickel acetate tetrahydrate [Ni$(CH_3COO)_2\cdot 4H_2O$, 99.5 %], 4,4′-bipyridine (BPY, 98 %) and 5-aminoisophthalic acid (AIP, 98 %) were all obtained from Aladdin Co., ltd.

2.2. Synthesis of Co-AIP-BPY and Ni-AIP-BPY

Co-AIP-BPY was synthesized according to previous literature [32]. In a typical procedure, $Co(CH_3COO)_2\cdot 4H_2O$ (2.298 g, 9.2 mmol) was dissolved with 80 mL deionized water in a beaker, and 4,4′-bipyridine (0.624 g, 4.0 mmol) and 5-aminoisophthalic (1.450 g, 8.0 mmol) were mixed with 80 mL methanol. Then, the above two solutions were mixed in a 200 mL Teflon-lined autoclave. After sonicating until homogenous, the mixture was finally heated at 60 °C for 72 h. Deionized water and methanol were used to wash the final collected purple powder, and then the solvent exchange of the as-synthesized sample was performed by using methanol for 3 days. The preparation method of Ni-AIP-BPY was the same as that of Co-AIP-BPY, except that $Ni(CH_3COO)_2\cdot 4H_2O$ was used instead of $Co(CH_3COO)_2\cdot 4H_2O$, and the green powder was finally collected. Activated Co-AIP-BPY and Ni-AIP-BPY were obtained by heating under vacuum at 200 °C for 8 h.

2.3. Characterization methods

The powder X-ray diffraction (PXRD) patterns were collected on a PANalytical X'Pert PRO X-ray diffractometer (Cu-Kα radiation, λ = 1.54059 Å) operating at 40 kV and 40 mA, and the scanning speed was 5°/min. Scanning electron microscopy (SEM) images were taken on a Hitachi TM 3000 scanning electron microscope. Fourier transform infrared spectroscopy (FTIR) analysis was carried out on a Bruker Vertex-70 spectrophotometer. Thermogravimetric analyses (TGA) were performed on an SDT Q600 (TA Instruments-Waters LLC, USA) from ambient temperature to 800 °C under a N_2 atmosphere (100 mL/min). CO_2 adsorption isotherms were measured on a Micromeritics ASAP2050 system at 0 °C. C element analyses were measured on EMIA-8100H, and the N and H element analyses were measured on EMGA-930. The contact angle was measured on DSA100 through drop shape analysis.

2.4. Gas adsorption experiments

Single component N_2 and O_2 adsorption isotherms of Co-AIP-BPY and Ni-AIP-BPY were measured on a Micromeritics ASAP2050 system at 15, 20, and 25 °C with pressures up to 505 kPa. All samples were activated under vacuum at 200 °C for 8 h to remove the guest molecules methanol and water. N_2 and O_2 with a high purity of 99.999 % were used without any purification.

2.5. Adsorption theories

The single component N_2 and O_2 adsorption isotherms at 15, 20, and 25 °C were all fitted by the Langmuir model [33], which was used to calculate the IAST selectivity and the isosteric heat of adsorption. The Langmuir model equation can be expressed as follows:

$$q = \frac{q_m bp}{1 + bp} \quad (1)$$

where q is the amount of N_2 or O_2 adsorbed in equilibrium (mmol/g); q_m is the saturation capacity (mmol/g); b is the affinity coefficient; and p is the total pressure (kPa) of the bulk gas in equilibrium with the adsorbed phase.

The O_2/N_2 selectivity was calculated from the single component N_2 and O_2 adsorption isotherms according to ideal adsorption solution theory (IAST) [34]. The final adsorption selectivity of O_2 to N_2 was calculated as follows:

$$S_{1/2} = \frac{x_{O_2}/y_{O_2}}{x_{N_2}/y_{N_2}} \quad (2)$$

where x_{O_2} and x_{N_2} are the mole fractions of O_2 and N_2 in the adsorbed phase, respectively, and y_{O_2} and y_{N_2} are the mole fractions of O_2 and N_2 in the gas phase, respectively.

The isosteric heat of adsorption (Q_{st}) was calculated based on the Clausius-Clapeyron equation [25,35]:

$$\ln(P) = \left(\frac{-Q_{st}}{R}\right)\left(\frac{1}{T}\right) + C \quad (3)$$

The slope of ln(P) versus 1/T at each loading was calculated to obtain the Q_{st}.

2.6. Breakthrough experiments

Breakthrough experiments were performed on a home-assembly experimental setup (Fig. S1) [36] and carried out with a binary mixture of O_2/N_2 (21/79, v/v). The adsorption column (stainless steel, diameter = 8 mm, length = 30 cm) was packed with 6 g pelleted sample. Breakthrough experiments were performed at 25 °C and 100 kPa for feed gas flowing at 10 mL/min, then the desorption curves were recorded through switching to purge gas (He). After breakthrough, the adsorbent was regenerated in situ by flowing pure He (60 mL/min) through the column with a residence time of 10 min.

2.7. Molecular simulation details

The interaction energies between N_2/O_2 and MOFs were calculated by the Materials Studio software, CASTEP module. The Generalized Gradient Approxi-mation (GGA), Perdew-Berke-Ernzernhof (PBE) functional within the Density functional theory (DFT) was used to optimize all structures [37]. The set optimization convergence standard SCF tolerance value was 0.01 meV/atom. A cutoff energy of 600 eV was installed at the same time. The single-point energy of optimized N_2 and O_2 molecules was calculated by placing N_2 and O_2 molecules, respectively, into a unit cell with the same cell dimensions as the Co-AIP-BPY or Ni-AIP-BPY primitive unit cell. The final structures after adsorbing N_2 or O_2 were prepared by placing one N_2 or O_2 molecule at a distance of approximately 2 Å from the metal site. The charge density difference upon N_2 and O_2 adsorption was analyzed based on the final structure after introducing the guest molecule and optimizing structure. The interaction energies between N_2/O_2 and the MOF sorbents and the difference between them were calculated as:

$$IE(N_2) = E(MOF + N_2) - E(MOF) - E(N_2) \quad (4)$$

$$IE(O_2) = E(MOF + O_2) - E(MOF) - E(O_2) \quad (5)$$

$$\Delta E = IE(N_2) - IE(O_2) \quad (6)$$

where $IE(N_2)$ and $IE(O_2)$ are the interaction energies between N_2/O_2 and MOFs; $E(MOF + N_2)$ and $E(MOF + O_2)$ are the total energy of the optimized MOF-gas complex; $E(MOF)$, $E(N_2)$ and $E(O_2)$ are the single-point energy of MOFs, N_2 and O_2, respectively; and ΔE is the difference between $IE(N_2)$ and $IE(O_2)$.

3. Result and discussion

3.1. Structure characterization

Co-AIP-BPY was synthesized by the literature method, and using the same synthetic procedure except replacing $Co(CH_3COO)_2{\cdot}4H_2O$ with $Ni(CH_3COO)_2{\cdot}4H_2O$, Ni-AIP-BPY can be obtained. Co-AIP-BPY and Ni-AIP-BPY are isostructural [38]. As shown in Fig. 1a, each Co(II) or Ni(II) atom is located in a distorted octahedral coordination center, the carboxyl groups of two different AIP ligands provide three coordination sites, the amino group of one of AIP and the N atom of BPY provide the other two coordination sites, and the last axial coordination site is occupied by a water molecule. Based on this rule, each AIP and BPY is connected to three and two metal atoms, respectively, from an infinitely extending two-dimensional network. This two-dimensional network is further connected by hydrogen bonds between amino groups and carboxylate groups to become a three-dimensional supramolecular framework (Fig. 1b). After activation treatment, the coordinated water molecules in the axial direction can be removed, resulting in the formation of coordinatively unsaturated metal Co and Ni sites. As shown in Fig. 1c, the PXRD pattern results showed that the as-synthesized Co-AIP-BPY and Ni-AIP-BPY have the same major diffraction peaks as those of the simulated structures, which indicates that these samples were successfully synthesized. After being granulated under 20 MPa by putting tablet press equipment or immersing in water for 7 days, the PXRD patterns of Co-AIP-BPY and Ni-AIP-BPY did not change compared with the as-synthesized samples (Fig. S2). In addition, these MOFs also have good stability in various organic solvents (ethanol, acetonitrile, N,*N*-dimethylformamide, 1,3,5-trimethylbenzene, 1,2-dichloroethane and cyclohexane), and the RXRD patterns of soaked Co-AIP-BPY and Ni-AIP-BPY are identical to the as-synthesized samples (Fig. S3). Moreover, as shown in Fig. S4, the major diffraction peaks of Co-AIP-BPY and Ni-AIP-BPY soaked in HCl and NaOH aqueous solutions with pH values ranging from 2 to 12 were well-maintained. The above PXRD results all indicated that these MOFs materials have good structural and chemical stability. The results of contact angle analysis indicated that these MOFs are hydrophilic, and Ni-AIP-BPY is more hydrophilic than Co-AIP-BPY (Fig. S6). Based on the PXRD pattern and elemental analysis results (Table S1), we think that the lower crystallinity and higher C content of Co-AIP-BPY are the main reasons why it is more hydrophobic than Ni-AIP-BPY. The TGA curves (Fig. S11) showed that the structures of Co-AIP-BPY and Ni-AIP-BPY have high thermal stability up to 400 °C, and the weight loss stages near 120–150 °C belonged to the release of solvent methanol and coordinated water molecules, which is consistent with the literature [38]. It is worth noting that the N_2 adsorption capacities of these materials are very low at −196 °C, and the CO_2 adsorption isotherms at 0 °C can prove the maintenance of their pore structures.

3.2. N_2 and O_2 adsorption isotherms and IAST O_2/N_2 selectivities

To investigate the N_2 and O_2 adsorption performance of these adsorbents, we measured the single-component N_2 and O_2 adsorption isotherms of activated Co-AIP-BPY and Ni-AIP-BPY at 25 °C and pressures up to 505 kPa. As shown in Fig. 2, the N_2 uptakes on Co-AIP-BPY and Ni-AIP-BPY at 505 kPa were 0.23 mmol/g and 0.27 mmol/g, respectively. However, their O_2 uptakes were 0.43 mmol/g and 0.44 mmol/g, respectively, which are significantly higher than their N_2 uptakes. In addition, it is worth noting that the O_2 uptakes of Co-AIP-BPY and Ni-AIP-BPY continued to increase linearly with pressure, which is not like some MOFs that strongly bind to O_2: their O_2 adsorption isotherms rise sharply under very low pressure. This means that the interactions between Co-AIP-BPY/Ni-AIP-BPY and O_2 are not strong, which is beneficial to their regeneration at ambient temperature. The Langmuir model was used to fit the N_2 and O_2 single-component adsorption isotherms of Co-AIP-BPY and Ni-AIP-BPY, and the fitting parameters and correlation coefficients (R^2) are listed in Table S2. Then, the IAST method was used to calculate their O_2/N_2 selectivities. As shown in Fig. 2c, we found that the O_2/N_2 selectivities of Co-AIP-BPY (1.8, at 500 kPa) and Ni-AIP-BPY (1.6, at 500 kPa) at 25 °C were both significantly greater than 1 in the calculated pressure range, which also indicates that these adsorbents selectively adsorb O_2 over N_2 even in a

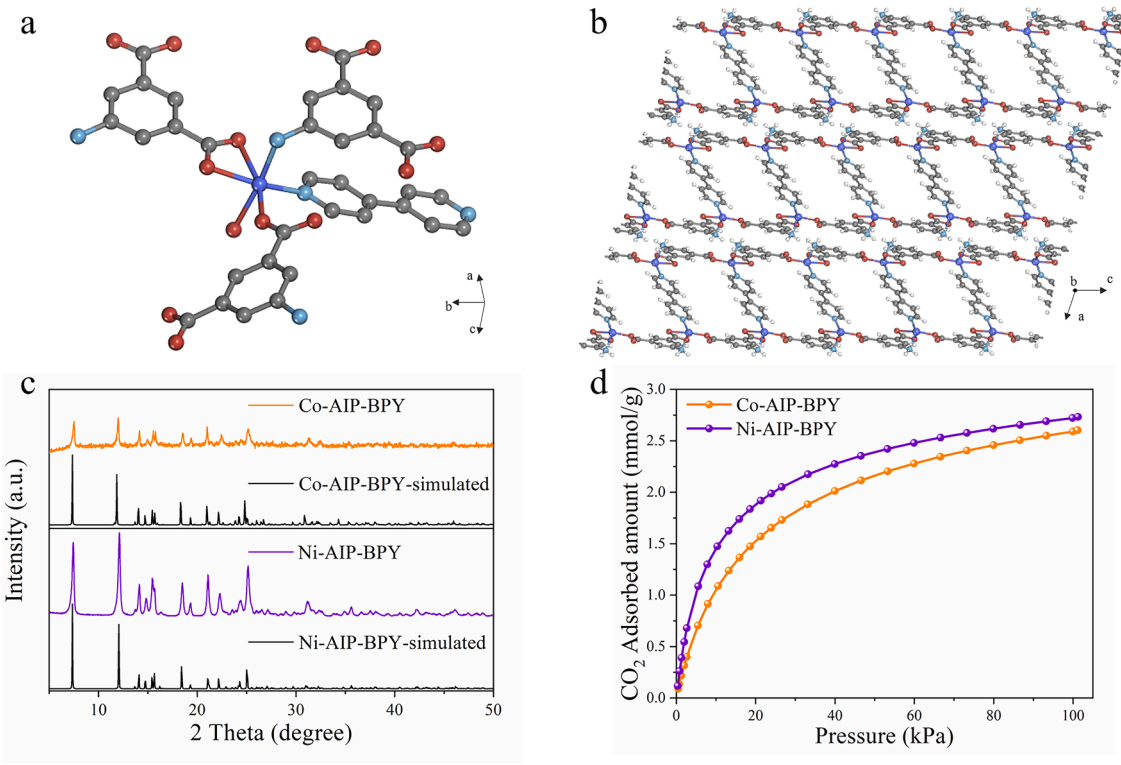

Fig. 1. (a) The coordination environment of the M(II) site in M−AIP−BPY (H atoms are omitted for clarity, Ni or Co, purple; O, red; C, gray; N, light blue). (b) View of the 1D channel of M−AIP−BPY along the b axis. (c) The PXRD patterns of as-synthesized Co-AIP-BPY and Ni-AIP-BPY and their simulated results. (d) The CO_2 adsorption isotherms of Co-AIP-BPY and Ni-AIP-BPY at 0 °C. (For interpretation of the references to colour in this figure legend, the reader is referred to the web version of this article.)

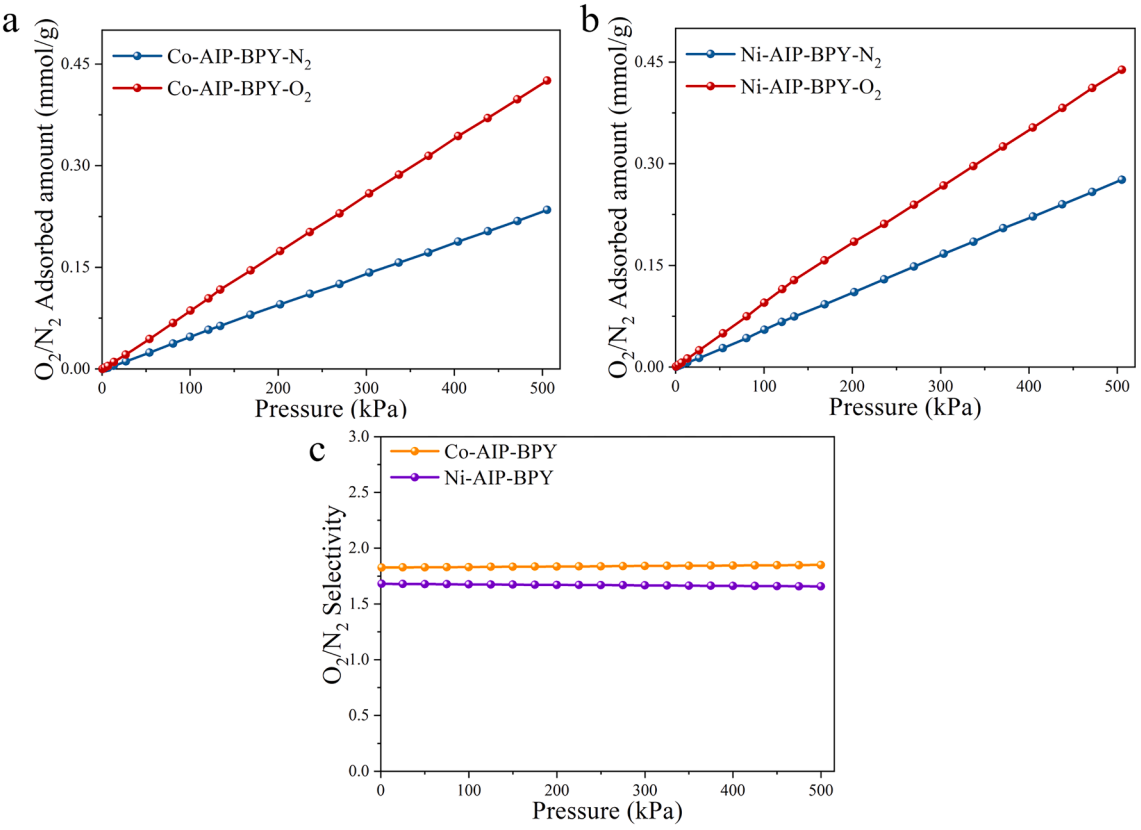

Fig. 2. N_2 and O_2 adsorption isotherms of (a) Co-AIP-BPY and (b) Ni-AIP-BPY at 25 °C and pressures up to 505 kPa. (c) IAST-predicted selectivities for the O_2/N_2 mixture (21/79, v/v) on Co-AIP-BPY and Ni-AIP-BPY at 25 °C.

mixed-component system. In addition, Co-AIP-BPY and Ni-AIP-BPY both have excellent framework stability. As shown in Fig. S12, there was almost no loss of N_2 and O_2 adsorption capacities after granulation (under 20 MPa) or immersion in water for 7 days, which is very advantageous in practical applications.

3.3. Isosteric heats of adsorption and O_2 adsorption–desorption cycles

Based on the above single-component adsorption isotherms and IAST-predicted results, we presume that the interactions between these adsorbents and O_2 are stronger than those with N_2. To further verify this inference, the Clausius-Clapeyron equation was used to calculate the isosteric heats of adsorption (Q_{st}) based on the Langmuir fitted N_2 and O_2 single-component adsorption isotherms at 15, 20 and 25 °C of adsorbents (Fig. S13). Fig. 3 show that the isosteric heats of O_2 adsorption on Co-AIP-BPY and Ni-AIP-BPY are both higher than that of N_2, which suggests that the frameworks of Co-AIP-BPY and Ni-AIP-BPY have stronger interactions with O_2 than with N_2. The above isosteric heat results further confirmed that Co-AIP-BPY and Ni-AIP-BPY are O_2-selective adsorbents. In addition, it is noteworthy that compared with some MOFs that have high initial O_2 isosteric heats (Q_{st} greater than 40 kJ/mol) [25,39], the isosteric heats of O_2 adsorption on Co-AIP-BPY and Ni-AIP-BPY are relatively low, which suggests that their desorption and regeneration will consume less energy and become easier.

To verify the regeneration performance of adsorbents, we performed five successive O_2 adsorption–desorption cycles for Co-AIP-BPY and Ni-AIP-BPY at 25 °C and pressures up to 505 kPa. For each cycle, the desorption step was carried out just by reducing the pressure to a certain vacuum condition at ambient temperature. As shown in Fig. 4, the O_2 adsorption capacities of Co-AIP-BPY and Ni-AIP-BPY were maintained well during five adsorption–desorption cycles, which demonstrates that the adsorption of O_2 on Co-AIP-BPY and Ni-AIP-BPY is reversible. This excellent regeneration performance of adsorbents at ambient temperature is attributed to the relatively low isosteric heats of O_2 adsorption on them. The results of adsorption heats and O_2 adsorption–desorption cycles on these adsorbents proved their O_2/N_2 separation potential once again. Table S3 lists the selectivities and regeneration abilities of some currently reported MOFs with O_2-selective adsorption properties. Most MOFs have good regeneration ability only at low temperatures, while the loss of adsorption capacities usually occurs at ambient temperature. Therefore, Co-AIP-BPY and Ni-AIP-BPY with complete regeneration ability at ambient temperature will have great advantages in application.

3.4. Dynamic O_2/N_2 breakthrough experiments

Breakthrough experiments with a binary mixture of O_2/N_2 (21/79, v/v) were performed at 25 °C and 100 kPa to investigate the dynamic O_2/N_2 separation performances of Co-AIP-BPY and Ni-AIP-BPY. As shown in Fig. 5a and 5b, N2 first eluted through the packed beds of Co-AIP-BPY and Ni-AIP-BPY in the breakthrough experiments, followed by the breakthrough of O_2 after reaching saturation, which indicates that these adsorbents adsorb more O_2 instead of N_2 in the dynamic process. In addition, the N_2 breakthrough curves of Co-AIP-BPY and Ni-AIP-BPY both showed roll-up effects, indicating that the initially adsorbed N_2 desorbs from the frameworks due to the competitive adsorption of O_2 [40]. Moreover, the breakthrough experiments desorption curves (Fig. S14) demonstrated that N_2 was desorbed faster than O_2 in the adsorption columns during the desorption process. These results all proved that Co-AIP-BPY and Ni-AIP-BPY have stronger interactions with O_2 than with N_2. It is worth noting that the regeneration of adsorbents can be simply achieved by flowing He at 25 °C. After three cycles, the O_2/N_2 separation performances of Co-AIP-BPY and Ni-AIP-BPY were still maintained (Fig. 5c and 5d), which is consistent with the static adsorption cycle results.

3.5. Adsorption mechanism

To investigate the O_2-selective adsorption and regeneration mechanism of Co-AIP-BPY and Ni-AIP-BPY, the density functional theory (DFT) method was used to analyze the charge density difference upon N_2 and O_2 adsorption in coordinatively unsaturated Co(II) and Ni(II) sites of M−AIP−BPY and calculate the interaction energies (IEs) between adsorbents and adsorbates. Fig. 6 presents the optimized adsorption configurations of Co-AIP-BPY and Ni-AIP-BPY after adsorbing N_2/O_2 and the charge density difference upon N_2 and O_2 adsorption. The yellow surfaces upon adsorbates represent a gain of electron density, and cyan surfaces represent a loss of electron density. After optimizing the adsorption configurations, the gain of electron density upon O_2 adsorption in Co-AIP-BPY and Ni-AIP-BPY was more significant than that of N_2, indicating that the electron transfers between the coordinatively unsaturated metal sites of adsorbents and O_2 were more obvious than that of N_2. These results further proved that the coordinated unsaturated transition metal sites of adsorbents are the main reason to make them selectively adsorb O_2 instead of N_2.

The results regarding the interaction energies (IEs) between the adsorbents and adsorbates are shown in Fig. 7. As a comparison, calculations of M−MOF−74 and M−BTTri (M = Co or Ni) were also carried out. In Fig. 7a, we compared and analyzed the difference in IEs between

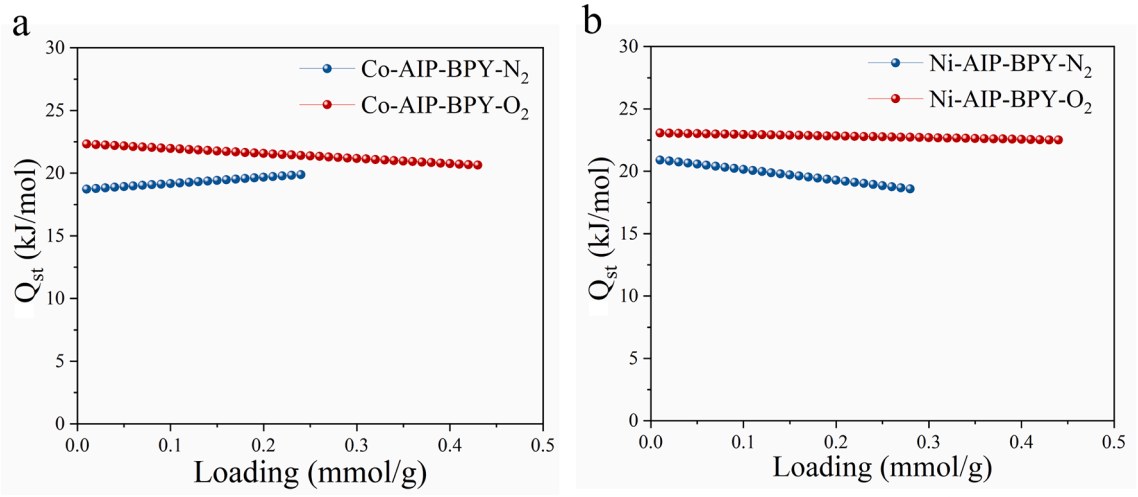

Fig. 3. Isosteric heats of N_2 and O_2 adsorption on (a) Co-AIP-BPY and (b) Ni-AIP-BPY.

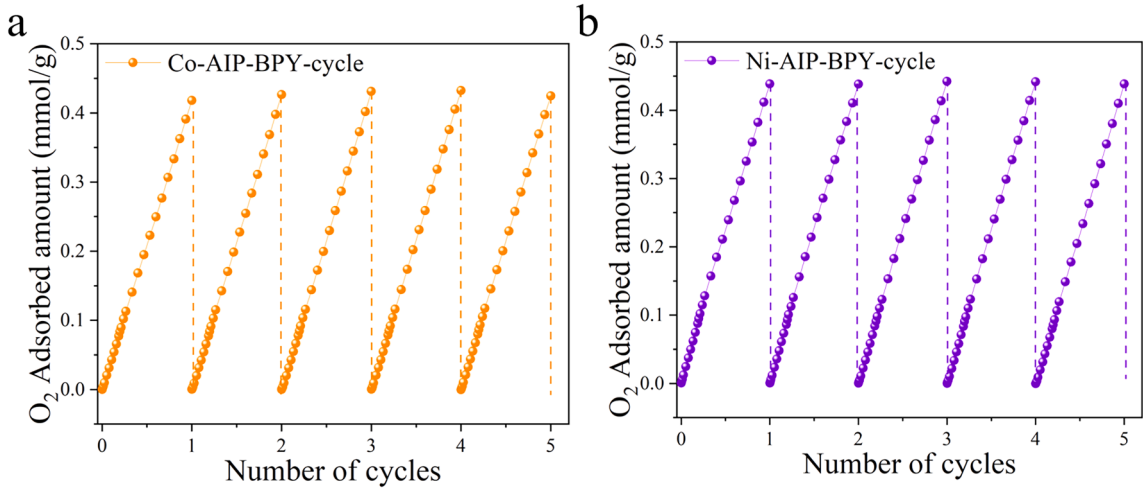

Fig. 4. The cyclic regeneration O_2 adsorption isotherms on (a) Co-AIP-BPY and (b) Ni-AIP-BPY.

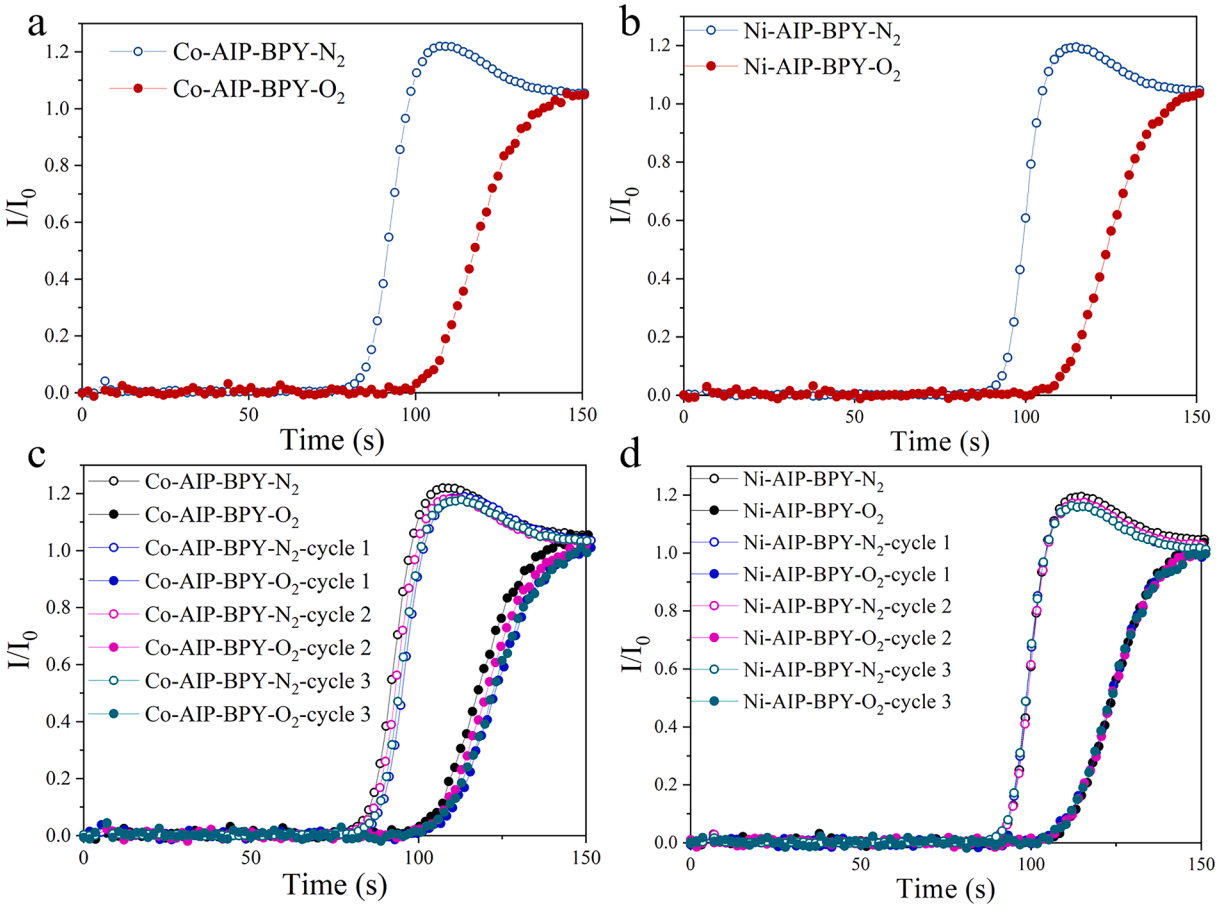

Fig. 5. Breakthrough curves of O_2/N_2 mixed gas (21/79, v/v) on (a) Co-AIP-BPY and (b) Ni-AIP-BPY at 25 °C and 100 kPa. Breakthrough cycle curves of O_2/N_2 mixed gas (21/79, v/v) on (c) Co-AIP-BPY and (d) Ni-AIP-BPY at 25 °C and 100 kPa.

M−AIP−BPY and M−MOF−74. It can be seen that the IE(O_2) of M−AIP−BPY is similar to the IE(O_2) of M−MOF−74, but the IE(N_2) of M−AIP−BPY is much higher than the IE(N_2) of M−MOF−74. The difference between IE(N_2) and IE(O_2), denoted ΔE, can clearly illustrate these results. A larger value of ΔE means that the difference between IE (N_2) and IE(O_2) is greater; it also indicates a greater difference between the N_2 and O_2 adsorption capacities of adsorbents. We found that the ΔE values of M−AIP−BPY are both larger than those of M−MOF−74, which indicates that M−AIP−BPY has a stronger ability to preferentially adsorb O_2 than N_2. M−MOF−74 hardly exhibits O_2 selectivity at ambient temperature because of its relatively low ΔE. In addition, compared with M−BTTri in Fig. 7b, the ΔE of M−AIP−BPY is similar to their ΔE, but the IE(O_2) of M−BTTri is more negative than that of M−AIP−BPY. These results indicated that the interactions between M−BTTri and O_2 are stronger than those of M−AIP−BPY; thus, it is difficult to desorb. This is why M−BTTri needs to be heated for

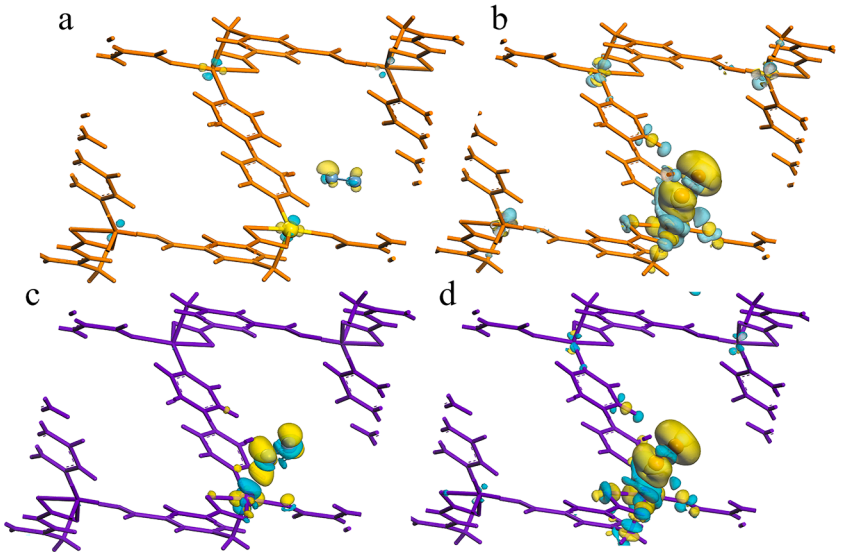

Fig. 6. The optimized configurations and the charge density difference upon (a) N_2 and (b) O_2 adsorption in Co-AIP-BPY. The optimized configurations and the charge density difference upon (c) N_2 and (d) O_2 adsorption in Ni-AIP-BPY. Isosurface value = 0.01 e^-/bohr^3.

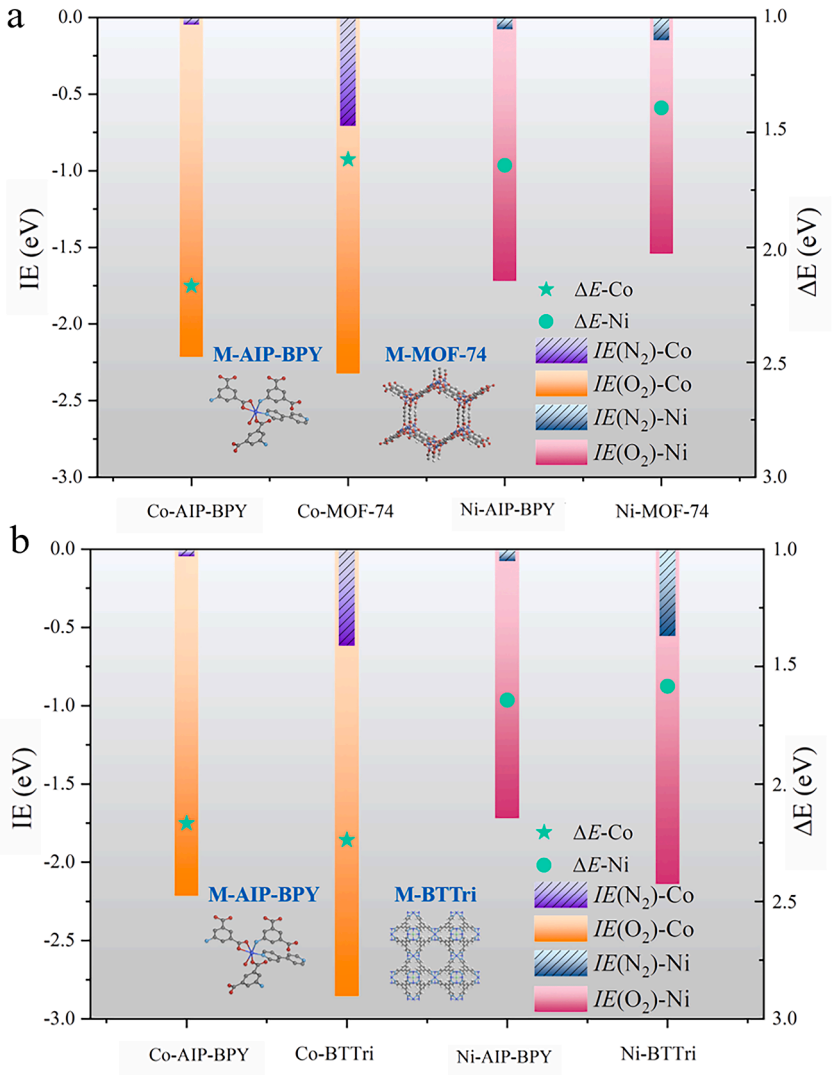

Fig. 7. The interaction energies (IEs) between different adsorbents and N_2 or O_2 and the difference (ΔE) between their IE(N_2) and IE(O_2).

regeneration after adsorbing O_2 at low temperature [25], while M−AIP−BPY can regenerate without any heat treatment processes.

4. Conclusions

In conclusion, we reported two O_2-selective adsorption mixed-ligand MOFs, Co-AIP-BPY and Ni-AIP-BPY, containing coordinated unsaturated metal sites Co(II) and Ni(II), which exhibit effective O_2-selective adsorption and regeneration performances at ambient temperature. The single-component N_2 and O_2 adsorption isotherms at 25 °C showed that they both have greater O_2 uptakes than N_2, and the IAST O_2/N_2 selectivities of Co-AIP-BPY and Ni-AIP-BPY were 1.8 and 1.6 at 25 °C and 500 kPa, respectively. Furthermore, the higher isosteric heats of O_2 adsorption on adsorbents compared with those of N_2 suggested that their frameworks have stronger interactions with O_2 than with N_2. Their relatively low O_2 adsorption heats indicated that their regeneration will become easy at the same time, which was revealed by five cycles of O_2 adsorption–desorption experiments. In addition, the breakthrough results demonstrated the excellent dynamic O_2/N_2 separation and regeneration performances of these MOFs. DFT theoretical calculations revealed the reasons for their O_2-selective adsorption capacity and excellent reproducibility. Due to the coordinated unsaturated Co(II) and Ni(II) sites and the unique ligands of Co-AIP-BPY and Ni-AIP-BPY, these MOFs have much stronger interactions with O_2 than with N_2. This work provides a meaningful strategy for searching and synthesizing suitable MOFs containing coordinated unsaturated sites to selectively adsorb O_2.

Declaration of Competing Interest

The authors declare that they have no known competing financial interests or personal relationships that could have appeared to influence the work reported in this paper.

Data availability

Data will be made available on request.

Acknowledgment

This work was supported by the Talent Program for Revitalization of Liaoning Province (XLYC1905017).

Appendix A. Supplementary data

Supplementary data to this article can be found online at https://doi.org/10.1016/j.cej.2022.138214.

References

[1] R.T. Yang, Adsorbents - fundamentals and applications, Wiley, New York, 2003.
[2] M.A. Habib, M. Nemitallah, R. Ben-Mansour, Recent Development in Oxy-Combustion Technology and Its Applications to Gas Turbine Combustors and ITM Reactors, Energy Fuels 27 (2013) 2–19.
[3] S. Shimomura, M. Higuchi, R. Matsuda, K. Yoneda, Y. Hijikata, Y. Kubota, Y. Mita, J. Kim, M. Takata, S. Kitagawa, Selective sorption of oxygen and nitric oxide by an electron-donating flexible porous coordination polymer, Nat. Chem. 2 (2010) 633–637.
[4] W.F. Castle, Air separation and liquefaction: recent developments and prospects for the beginning of the new millennium, Int. J. Refrig. 25 (2002) 158–172.
[5] N.D. Hutson, S.U. Rege, R.T. Yang, Mixed cation zeolites: LixAgy-X as a superior adsorbent for air separation, AIChE J. 45 (1999) 724–734.
[6] M.W. Ackley, S.U. Rege, H. Saxena, Application of natural zeolites in the purification and separation of gases, Microporous Mesoporous Mater. 61 (2003) 25–42.
[7] S.P. Nandi, P.L. Walker, SEPARATION OF OXYGEN AND NITROGEN USING 5A ZEOLITE AND CARBON MOLECULAR-SIEVES, Sep. Sci. 11 (1976) 441–453.
[8] S.A. Peter, J. Sebastian, R.V. Jasra, Adsorption of nitrogen, oxygen, and argon in mono-, di-, and trivalent cation-exchanged zeolite mordenite, Ind. Eng. Chem. Res. 44 (2005) 6856–6864.
[9] G. Sethia, R.S. Pillai, G.P. Dangi, R.S. Somani, H.C. Bajaj, R.V. Jasra, Sorption of Methane, Nitrogen, Oxygen, and Argon in ZSM-5 with different SiO_2/Al_2O_3 Ratios: Grand Canonical Monte Carlo Simulation and Volumetric Measurements, Ind. Eng. Chem. Res. 49 (2010) 2353–2362.
[10] Y. Tang, X. Wang, Y. Wen, X. Zhou, Z. Li, Oxygen-Selective Adsorption Property of Ultramicroporous MOF $Cu(Qc)_2$ for Air Separation, Ind. Eng. Chem. Res. 59 (2020) 6219–6225.
[11] H. Juntgen, K. Knoblauch, K. Harder, CARBON MOLECULAR-SIEVES - PRODUCTION FROM COAL AND APPLICATION IN GAS SEPARATION, Fuel 60 (1981) 817–822.
[12] T.R. Gaffney, Porous solids for air separation, Curr. Opin. Solid State Mater. Sci. 1 (1996) 69–75.
[13] N.D. Hutson, R.T. Yang, Synthesis and characterization of the sorption properties of oxygen-binding cobalt complexes immobilized in nanoporous materials, Ind. Eng. Chem. Res. 39 (2000) 2252–2259.
[14] D. Chen, A.E. Martell, Dioxygen affinities of synthetic cobalt schiff-base complexes, Inorg. Chem. 26 (1987) 1026–1030.
[15] A. Jayaraman, R.T. Yang, S.H. Cho, T.S.G. Bhat, V.N. Choudary, Adsorption of nitrogen, oxygen and argon on Na-CeX zeolites, Adsorption 8 (2002) 271–278.
[16] H. Liu, D. Yuan, G. Liu, J. Xing, Z. Liu, Y. Xu, Oxygen-selective adsorption on high-silica LTA zeolite, Chem. Commun. 56 (2020) 11130–11133.
[17] P. Krokidas, S. Moncho, E.N. Brothers, I.G. Economou, Defining New Limits in Gas Separations Using Modified ZIF Systems, ACS Appl. Mater. Interfaces 12 (2020) 20536–20547.
[18] S. Ma, X.-S. Wang, C.D. Collier, E.S. Manis, H.-C. Zhou, Ultramicroporous metal-organic framework based on 9,10-anthracenedicarboxylate for selective gas adsorption, Inorg. Chem. 46 (2007) 8499–8501.
[19] J.W. Yoon, S.H. Jhung, Y.K. Hwang, S.M. Humphrey, P.T. Wood, J.-S. Chang, Gas-sorption selectivity of CUK-1: A porous coordination solid made of cobalt(II) and pyridine-2,4-dicarboxylic acid, Adv. Mater. 19 (2007) 1830–1834.
[20] L. Kan, L. Li, G. Li, L. Zhang, Y. Liu, Three stable dinuclear M-2(OH)(0.5)(NO3)(0.5)(RCOO)(2)(RN)(4) (M = Cu, Ni) based metal-organic frameworks with high CO2 adsorption and selective separation for O-2/N-2 and C3H8/CH4, Inorg. Chem. Front. 7 (2020) 731–736.
[21] S. Yao, D. Wang, Y. Cao, G. Li, Q. Huo, Y. Liu, Two stable 3D porous metal-organic frameworks with high performance for gas adsorption and separation, J. Mater. Chem. A 3 (2015) 16627–16632.
[22] I.B. Orhan, H. Daglar, S. Keskin, T.C. Le, R. Babarao, Prediction of O-2/N-2 Selectivity in Metal-Organic Frameworks via High-Throughput Computational Screening and Machine Learning, ACS Appl. Mater. Interfaces 14 (2022) 736–749.
[23] H. Demir, S.J. Stoneburner, W. Jeong, D. Ray, X. Zhang, O.K. Farha, C.J. Cramer, J. I. Siepmann, L. Gagliardi, Metal-Organic Frameworks with Metal-Catecholates for O-2/N-2 Separation, J. Phys. Chem. C 123 (2019) 12935–12946.
[24] E.D. Bloch, L.J. Murray, W.L. Queen, S. Chavan, S.N. Maximoff, J.P. Bigi, R. Krishna, V.K. Peterson, F. Grandjean, G.J. Long, B. Smit, S. Bordiga, C.M. Brown, J.R. Long, Selective Binding of O_2 over N_2 in a Redox-Active Metal-Organic Framework with Open Iron(II) Coordination Sites, J. Am. Chem. Soc. 133 (2011) 14814–14822.
[25] D.J. Xiao, M.I. Gonzalez, L.E. Darago, K.D. Vogiatzis, E. Haldoupis, L. Gagliardi, J. R. Long, Selective, Tunable O_2 Binding in Cobalt(II)-Triazolate/Pyrazolate Metal-Organic Frameworks, J. Am. Chem. Soc. 138 (2016) 7161–7170.
[26] A.S. Rosen, M.R. Mian, T. Islamoglu, H. Chen, O.K. Farha, J.M. Notestein, R. Q. Snurr, Tuning the Redox Activity of Metal-Organic Frameworks for Enhanced, Selective O_2 Binding: Design Rules and Ambient Temperature O_2 Chemisorption in a Cobalt-Triazolate Framework, J. Am. Chem. Soc. 142 (2020) 4317–4328.
[27] D.F. Sava Gallis, K.W. Chapman, M.A. Rodriguez, J.A. Greathouse, M.V. Parkes, T. M. Nenoff, Selective O_2 Sorption at Ambient Temperatures via Node Distortions in Sc-MIL-100, Chem. Mater. 28 (2016) 3327–3336.
[28] L.J. Murray, M. Dinca, J. Yano, S. Chavan, S. Bordiga, C.M. Brown, J.R. Long, Highly-Selective and Reversible O_2 Binding in Cr_3(1,3,5-benzenetricarboxylate)$_2$, J. Am. Chem. Soc. 132 (2010) 7856–7857.
[29] E.D. Bloch, W.L. Queen, M.R. Hudson, J.A. Mason, D.J. Xiao, L.J. Murray, R. Flacau, C.M. Brown, J.R. Long, Hydrogen Storage and Selective, Reversible O_2 Adsorption in a Metal-Organic Framework with Open Chromium(II) Sites, Angew. Chem. Int. Ed. 55 (2016) 8605–8609.
[30] M.H. Rosnes, D. Sheptyakov, A. Franz, M. Frontzek, P.D.C. Dietzel, P.A. Georgiev, On the elusive nature of oxygen binding at coordinatively unsaturated 3d transition metal centers in metal-organic frameworks, Phys. Chem. Chem. Phys. 19 (2017) 26346–26357.
[31] M.V. Parkes, D.F. Sava Gallis, J.A. Greathouse, T.M. Nenoff, Effect of Metal in $M_3(btc)_2$ and M_2(dobdc) MOFs for O_2/N_2 Separations: A Combined Density Functional Theory and Experimental Study, J. Phys. Chem. C 119 (2015) 6556–6567.
[32] H. Wu, Y. Yuan, Y. Chen, F. Xu, D. Lv, Y. Wu, Z. Li, Q. Xia, Efficient adsorptive separation of propene over propane through a pillar-layer cobalt-based metal-organic framework, AIChE J. 66 (2020).
[33] B.U. Choi, D.K. Choi, Y.W. Lee, B.K. Lee, S.H. Kim, Adsorption equilibria of methane, ethane, ethylene, nitrogen, and hydrogen onto activated carbon, J. Chem. Eng. Data 48 (2003) 603–607.
[34] A.L. Myers, J.M. Prausnitz, THERMODYNAMICS OF MIXED-GAS ADSORPTION, AIChE J. 11 (1965) 121–127.
[35] D. Lv, R. Shi, Y. Chen, Y. Wu, H. Wu, H. Xi, Q. Xia, Z. Li, Selective Adsorption of Ethane over Ethylene in PCN-245: Impacts of Interpenetrated Adsorbent, ACS Appl. Mater. Interfaces 10 (2018) 8366–8373.
[36] Y.Q. Wu, D.H. Yuan, D.W. He, J.C. Xing, S. Zeng, S.T. Xu, Y.P. Xu, Z.M. Liu, Decorated Traditional Zeolites with Subunits of Metal-Organic Frameworks for CH_4/N_2 Separation, Angew. Chem. Int. Ed. 58 (2019) 10241–10244.

[37] J.P. Perdew, K. Burke, M. Ernzerhof, Generalized gradient approximation made simple, Phys. Rev. Lett. 78 (1997) 1396.
[38] Y. Hu, W. Zhang, X. Zhang, Z. Wang, Y. Li, J. Bai, Two corrugated 2D bilayer (6^3)($6^5$8) topological coordination polymers: Synthesis, structure, and water-induced reversible transformation, Inorg. Chem. Commun. 12 (2009) 166–168.
[39] D.A. Reed, D.J. Xiao, H.Z.H. Jiang, K. Chakarawet, J. Oktawiec, J.R. Long, Biomimetic O-2 adsorption in an iron metal-organic framework for air separation, Chem. Sci. 11 (2020) 1698–1702.
[40] M. Chang, Y. Zhao, D. Liu, J. Yang, J. Li, C. Zhong, Methane-trapping metal-organic frameworks with an aliphatic ligand for efficient CH_4/N_2 separation, Sustainable, Energy Fuels 4 (2020) 138–142.